

Comparison between the Performance of Pulsed, Pulsed Phase and Pulsed Eddy Current Thermography Modalities Regarding to the Detection of Artificial Defects in CFRP with Machine Learning for Classification

by M. GROSSO LIMA*, I. B. C. de Paula**, R. M. Cautivo***, C. G. Camerini**** and G. R. Pereira*****

* Laboratory of Nondestructive Testing, Corrosion and Welding, Department of Metallurgical and Materials Engineering, Federal University of Rio de Janeiro, Rio de Janeiro, RJ, Brazil, marcellag@metalmat.ufrj.br

** Laboratory of Nondestructive Testing, Corrosion and Welding, Department of Metallurgical and Materials Engineering, Federal University of Rio de Janeiro, Rio de Janeiro, RJ, Brazil, ighorbarci@Indc.metalmat.ufrj.br

*** Laboratory of Nondestructive Testing, Corrosion and Welding, Department of Metallurgical and Materials Engineering, Federal University of Rio de Janeiro, Rio de Janeiro, RJ, Brazil, raquelmcautivo@Indc.metalmat.ufrj.br

*Department of Metallurgical and Materials Engineering, COPPE, Federal University of Rio de Janeiro, Rio de Janeiro, RJ, Brazil, cgcamerini@metalmat.ufrj

*Department of Metallurgical and Materials Engineering, COPPE, Federal University of Rio de Janeiro, Rio de Janeiro, RJ, Brazil, gpereira@metalmat.ufrj.br

Abstract

A CFRP specimen with inserted defects of different sizes and depths was evaluated by Pulsed Thermography (PT), Pulsed Phase Thermography (PPT) and Pulsed Eddy Current Thermography (PECT). In addition to the comparison of experimental results, which is relative to defect detection, the machine learning methodology was also used for binary classification of signals into defective and non-defective regions.

In addition to the analysis regarding the detection presented by each modality in relation to the size and depth of the defects, the results of applying supervised machine learning to the binary classification of temperature signals from PT and PECT modalities are discussed, considering metrics such as accuracy, precision and recall for the Support Vector Machine, Neural Networks and Ensemble models. The results indicate effective performance in defect detection, especially in class 1 (defective region), for both modalities.

1. Introduction

Over the last few years, thermography has attracted increasing attention as a non-destructive technique for the inspection of different types of materials [1-3]. In general, thermography can be divided into two categories: passive thermography and active thermography. Active thermography employs a variety of external heating sources to generate heat in the materials, such as light, eddy current, ultrasound, microwave [4,5]. The Pulsed Thermography (PT) and Pulsed Phase Thermography (PPT) use an optical excitation heat source and halogen lamps are generally used as an external source [6]. For the pulsed eddy current thermography (PECT), the heating mechanism involves inducing eddy current and then generating Joule heat in conductive materials, which makes it possible to detect defects within skin depth accurately and efficiently [7]. Some studies have already demonstrated the effectiveness of the PECT to detect defects in metallic materials [8,9,10], however, there are few studies carried out applying this technique to the inspection of CFRP (Carbon Fiber Reinforced Plastic) materials.

At the same time that non-destructive techniques have been increasingly improved to detect defects and guarantee the integrity of materials, new technologies area also being added to techniques both for data analysis and to assist in decision-making done by inspectors. Among these technologies, machine learning has become increasingly present in the post-processing and data analysis stages in Engineering, given that it can combine mathematical, statistical and programming tools in the use of algorithms intended for predictions of characteristics coming from information based on the analyzed data [11, 12]. In this study, supervised learning was chosen due to the following factors: the data obtained from the inspection could be associated with a label, clarity in binary classification (defect or non-defect) and versatility of algorithms. Considering that the area of machine learning comprises an extensive set of analysis methodologies resources, this study will cover in greater detail only the classification models evaluated in this study through supervised learning, namely: Random Forest (RF), Support Vector Machine (SVM), K Nearest Neighbor (KNN), Neural Network (RN) and Ensemble Learning.

Considering that knowledge of the detection limit of delamination defects in CFRP using the PECT technique is still a challenge and there is a great scarcity of studies related to this topic, this work proposes to investigate the feasibility of PECT to detect the delamination defect on CFRP within depths ranging from 0.31 mm to 4.03 mm. A comparative both in relation to the capacity of defect detection and also to the performance of the machine learning classifiers was carried out between the thermography modalities evaluated in this study.



2. Material and Methods

The CFRP specimen contains sixteen plies of carbon fiber fabric of 0.31 mm thickness each one. Its lateral dimensions are 340 mm x 300 mm for an overall thickness of 4.96 mm. The fiber orientations are 0° and the matrix is an epoxy. The specimen was fabricated by the prepreg process using a vacuum system. The artificial delamination defects were realized by inserting square Teflon tapes having lateral dimensions of 3 mm x 3 mm, 5 mm x 5 mm, 7 mm x 7 mm, 10 mm x 10 mm and 15 mm x 15 mm and thickness equal to 0.45 mm. The specimen contains defects that were inserted at depth: 0.31 (Line J), 0.93 (Line L), 1.55 (Line M), 2.17 (Line N), 2.79 (Line O), 3.41 (Line P) and 4.03 mm (Line Q), as depicted in Fig. 1.

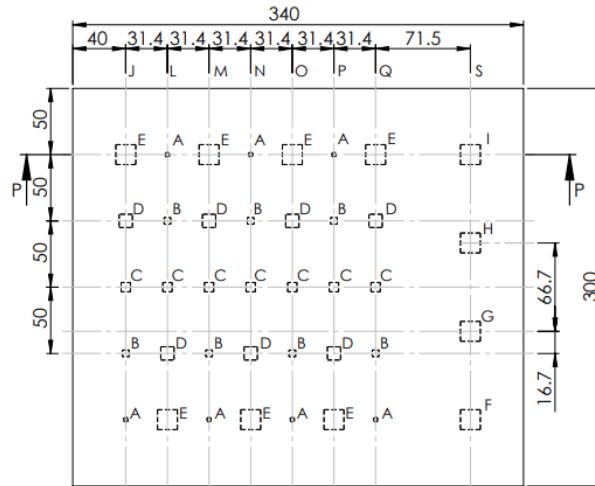


Fig. 1. Schematic diagram of the CFRP sample with artificial delamination defects evaluated in this study.

For the experimental tests, both for PECT and for PT and PPT, the infrared camera used was FLIR SC5600, which was a stirling cooled camera with 640 x 512 pixels of 2.5 – 5.1 μm InSb detectors and sensitivity of < 30 mK. The camera was controlled by a computer which allowed the capturing of thermal images with the same frame rate of the camera, 50 Hz, as well as the storage of a sequence containing 3000 thermograms.

The PECT tests were carried out with EASYHEAT 0224 (Ambrell Company, America) as an induction heating system and the infrared camera to record the thermal response on the sample surface. This setup is shown in Fig. 2. The induction heating system is composed of an energy power supply (maximum excitation power of 2.4 kW, maximum current of 400 A and an excitation frequency range of 150-400 kHz), a movable work head, a coil and a Flowmax 230 water-cooling system (protect the inductive coil from heating damage caused by the internal currents). Considering the geometry of the sample investigated in this study, a rectangular coil was constructed to perform the PECT tests.



Fig. 2. Photograph of the experimental setup used to carry out the PECT tests.

The experimental tests using optical mode heating (PT and PPT) was carried out with 3.4 kW halogen lamps to generate a 10 seconds of heat pulse on the sample surface. For these tests, the heat source was positioned on the same side of the sample with respect to the IR camera (reflection mode), as shown in Fig. 3.



Fig. 3. Photograph of the experimental setup used to carried out the PT and PPT tests.

For the machine learning methodology, the software chosen in this study to implement the codes was Python, version 3.10.11. In the implemented code, several libraries were used, including pandas, for efficient data manipulation; matplotlib for graphical visualization and scikit-learn for machine learning algorithms. The binary classification adopted in this study considered signals classified as intact (non-defect) as 0 and signals corresponding to defects as class 1. The input data in the models was the temperature over time obtained through the line profile in both PT and PECT. This tool is available in the thermal camera analysis software (Altair) and allows the parameter chosen by the user to be exported in text form (file). The input data was separated into two dataframe, the first corresponding to the training and testing data and the second, with the data to be used for validation. This way, the validation data will not be seen during the model training and testing process, that is, it will be new data to be inserted into the subsequent stage of learning. Another highlight to be mentioned in this implementation was the choice of 80% of the data from the first dataframe to be used in the training stage and 20% for testing. Table 1 presents the quantities of sample data inserted into the models according the thermography modalities evaluated and Fig. 5 and Fig. 6 show graphs illustrating the number of sample data for each step described above.

Table 1. Number of sample data used for the classification models according to the thermography modalities evaluated

	Class (Output)	Number of sample data
PT	0	733
	1	735
PECT	0	657
	1	660

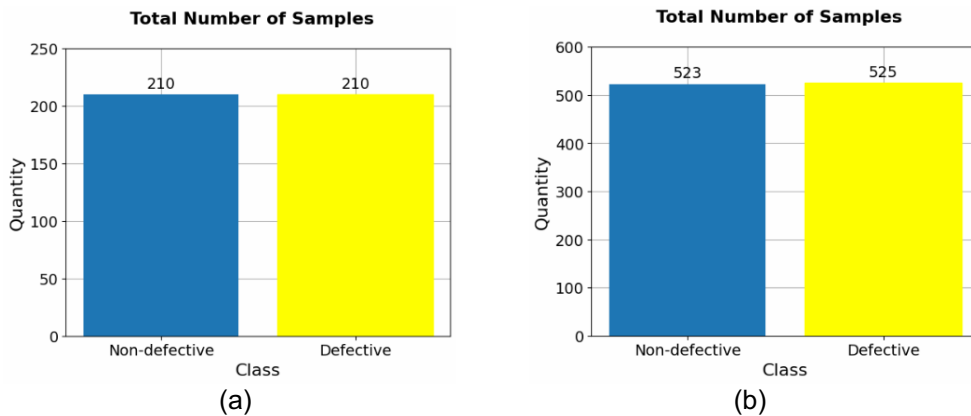


Fig. 4. Number of sample data per class used in the PT modality in the stage: (a) training/testing and (b) validation.

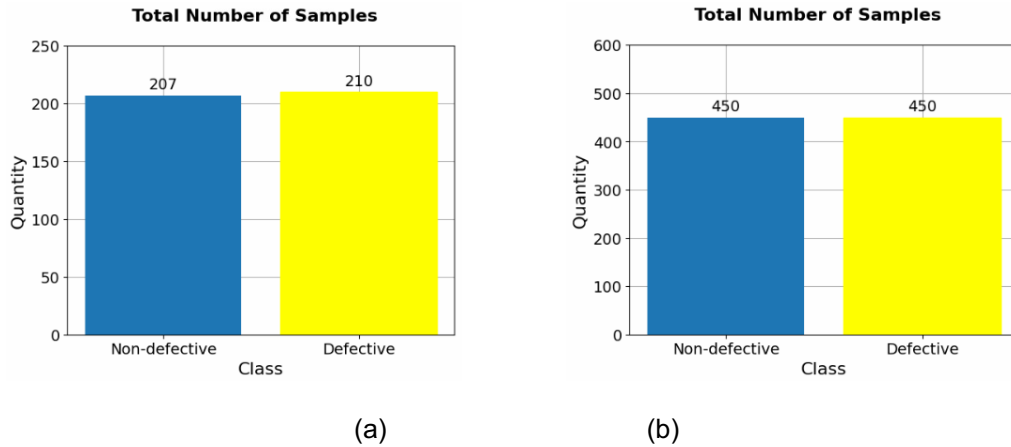


Fig. 5. Number of sample data per class used in the PECT modality in the stage: (a) training/testing and (b) validation.

3. Results and Discussion

For the PECT, the choice of the camera and coil positioning (transmission mode) was based on the volumetric heating presented by the CFRP sample and for this reason, the coil is not shown in the thermograms obtained. The results for PECT tests were presented in the form of a sequence of thermograms including the heating and cooling period of the sample. Considering that the defects were inserted at seven different depths (Fig.6), for each test carried out, the geometric center of the coil was positioned coincident with the geometric center of the defects for each depth. Thus, the first test was positioned with the coil centered on the defects of line J of the sample (depth of 0.31 mm), the second test with positioning of line L (depth of 0.93 mm) and so on. The thermogram with the best contrast obtained for each sequence and consequently for each test was chosen for analysis and is presented in Fig.6. Analyzing the thermogram, Fig. 6(a), corresponding the result obtained with the positioning of the coil centered in the region corresponding to the defects inserted on the 0.31 mm depth (Line J), it is possible to identify the three largest defects, being 15 x 15 mm, 10 x 10 mm and 7 x 7 mm in the vertical direction from top to bottom. Fig.6 (b) shows the result obtained with the positioning of the coil centered in the region corresponding to the defects inserted on the 0.93 mm depth (Line J) and once again the presence of the three largest defects can be observed. Positioning the coil centered on line M, whose depth of defects was 1.55 mm from the surface, according to the thermogram shown in Fig. 6(c), it is possible to see the presence of the three largest defects, located in the upper part of the sample. Furthermore, by comparing this result with that already presented in previous coil positions, a reduction in contrast level presented by the defects is observed, however this behavior is explained by the increase in the depth of defects and consequently a reduction in the intensity of the electrical currents that circulate around it and are responsible for the thermal induction. Fig. 6(d) shows the result obtained by positioning the center of the coil coincident with the Line N of defects (depth of 2.17 mm from the surface) and according to the thermogram obtained, only the two largest defects can be observed in the lower part of the sample. For tests with the positioning of the coil on lines O, P, Q, it was not possible to observe the presence of any of the defects and this behavior is explained by the depth of the defects being greater and the thermal contrast being very small.

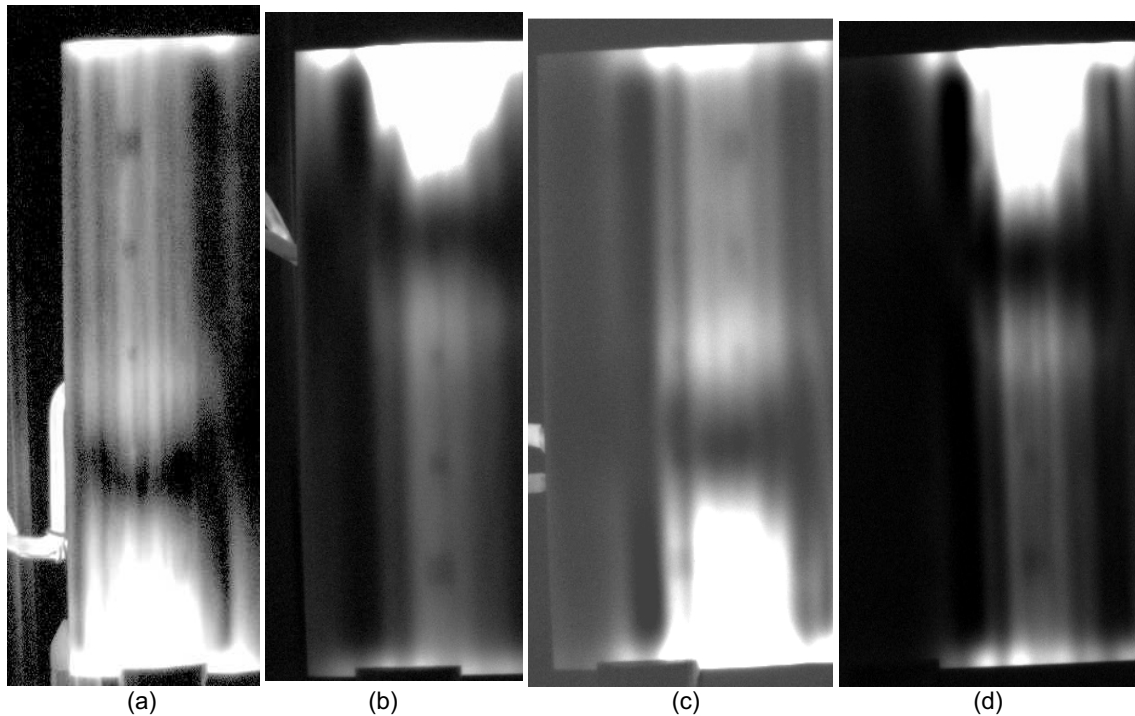


Fig. 6. Thermogram obtained by PECT with the positioning of the coil in the region where the defects are found at a depth of: (a) 0.31 mm (Line J), (b) 0.93 mm (Line L), (c) 1.55mm and (d) 2.17mm.

The highest contrast thermogram obtained in the PT modality sequence is shown in Fig. 7. Analyzing this result, it is possible to observe the detection of the 4 largest defects of depths 0.31, 0.93 and 1.55 (corresponding to lines J, L and M respectively). It was not possible to detect any defect positioned on the N line (depth of 2.17 mm), however in the PECT modality, as shown in Fig. 6 (b), the two largest defects were detected, even with low contrast.

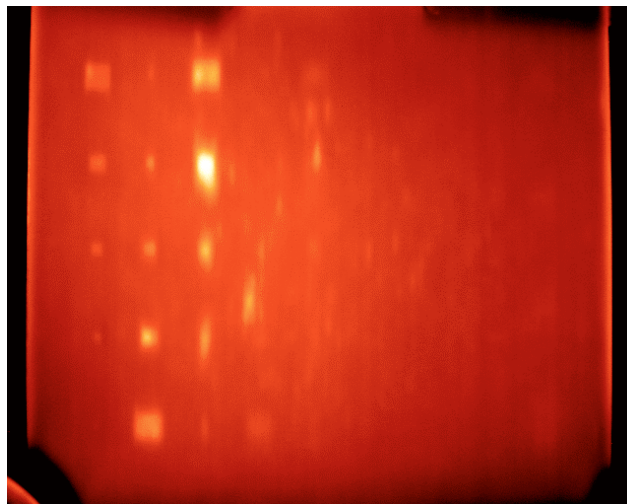


Fig. 7. Thermogram of the highest contrast of the TP sequence

In addition to the inspections carried out using the PT modality, this specimen was also inspected by PPT. This modality can be considered a post-processing of the data obtained from PT and its results are presented in the form of a phase image and an amplitude image. In Figure 42 the phase image is presented and comparing this result with that obtained by the previous modality, from the point of view of detecting defects, it was possible to observe the presence of the largest defect positioned at a depth of 2.17 mm (Line N), which was not observed in PT. In relation to defects detected at shallower depths, there was an improvement in the definition of their contours and noise reduction in the phase image.

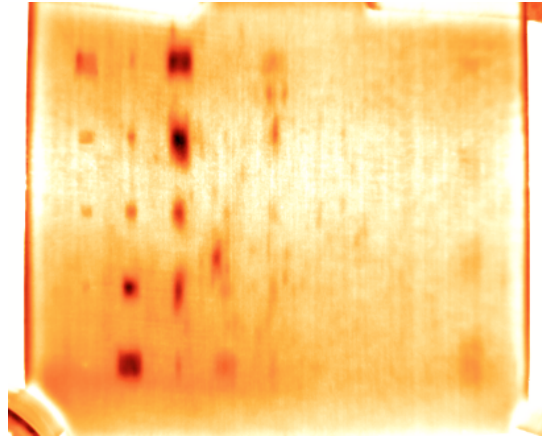


Fig. 8. Phase image obtained in the PPT test

In order to summarize the results obtained in relation to the detection of defects for each thermography modality, in Fig. 9 a schematic diagram is presented with the detected (in green) and undetected (in red) defects.

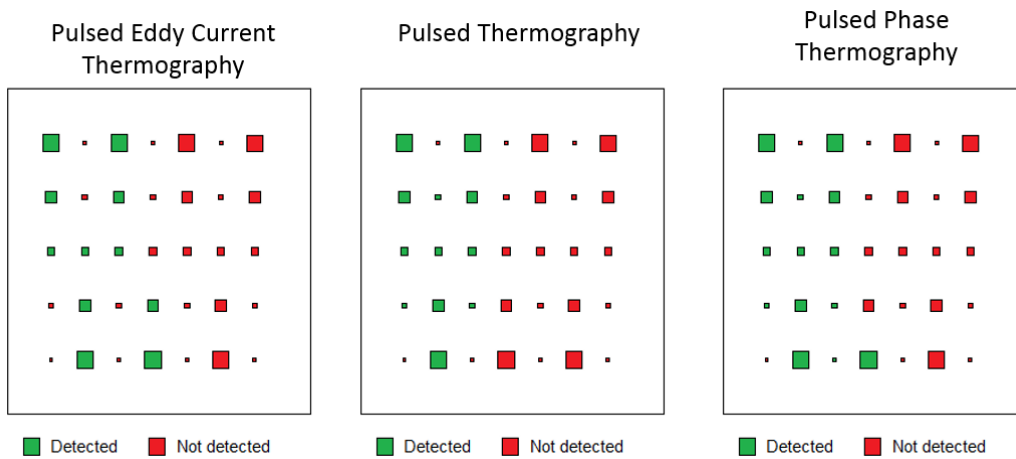


Fig. 9. Schematic diagram of the CFRP specimen with defects detected in green and non-detected defects in red for: (a) PECT, (b) PT and (c) PPT.

According to the literature review on studies using supervised machine learning in non-destructive tests, the following models were chosen for the binary classification of data: Support Vector Machine (SVM), Neural Network (NN) and Ensemble Learning. The performance of each classifier model was evaluated using the metrics of accuracy, precision and recall (sensitivity). The results obtained by the machine learning methodology in data classification are presented in Table 2. Analyzing these results, it is observed that both thermography modalities presented metrics that indicate good performance in data classification. However, the performance presented in the metrics is subtly superior with input data by PECT in relation to TP.

Table 2. Metrics used to evaluate the performance of classifiers with input data from the Pulsed Thermography (PT) and Pulsed Eddy Current Thermography (PECT)

Metrics	Classification Models					
	Pulsed Thermography (PT)			Pulsed Eddy Current Thermography (PECT)		
	SVM	NN	Ensemble	SVM	NN	Ensemble
Accuracy (%)	97,04	97,23	97,52	98,44	97,89	98,44
Precision (%)	98,00	98,00	98,00	98,00	98,00	98,00
Recall (%)	96,00	97,00	97,00	99,00	99,00	99,00

4. Conclusion

According to the results obtained, the PECT modality was able to detect defects inserted in the specimen simulating delamination larger than 7 mm (lateral size) and with depths up to 2.17 mm. This result is considered promising because in the literature there are very few studies dedicated to investigating the detection of defects deeper than 1 mm by PECT. Comparing these results with those presented by the PT and PPT modality, there was no increase in the depth of the already detected defects, but they were detected with greater contrast in the thermograms and the smallest defects at depth of 0.93 and 1.55 mm could be detected.

Regarding the proposed methodology for using supervised machine learning for binary classification of temperature over time, the results obtained for the models' studies were promising due to the high degree of accuracy in the samples, both for the PT as well PECT. Furthermore, this methodology also showed the best performance in classifying data from PECT in relation TP.

REFERENCES

- [1] Xu, C., Zhang, W., Wu, C., et al., "An improved method of eddy current pulsed thermography to detect subsurface defects in glass fiber reinforced polymer composites". *Composite Structures*, vol. 242, 2020.
- [2] Gao, B., Li, X., Woo, W.L., et al., Quantitative validation of Eddy current stimulated thermal features on surface crack, *NDT & E International*, v. 85, pp. 1 – 12, 2017.
- [3] Wilson, J., Tian, G., Mukriz, I., et al., PEC thermography for imaging multiple cracks from rolling contact fatigue, *NDT & E International*, v. 44, pp. 505-512, 2011.
- [4] Kidangan, R.T., Unnikrishnakurup, S., Krishnamurthy, C.V., et al., Induction thermography for unidirectional CFRP composites: A novel inspection approach trough global current path integration, *Composites Structures*, v. 327, 2024.
- [5] Yang, R., He, Y., Optically and non-optically excited thermography for composites: A review, *Infrared Physics & Technology*, v. 75, 2016.
- [6] Grosso, M., Soares, I. A., Lopez, J.E.C, et al. Study on the limit detection of defects by pulsed thermography in adhesive composite joints trough computational simulation, *Composites Part B: Engineering*, v. 168, 2019.
- [7] Tian, G. Y. et al. Pulsed eddy current thermography and applications. *New Developments in Sensing Technology for Structural Health Monitoring*, p. 205-231, 2011.
- [8] Tian, G. Y., Gao, Y., Li, K., et al., Eddy current pulsed thermography with different excitation configurations for metallic material and defect characterization, *Sensors*, v. 843, 2016.
- [9] Yang, S., Tian, G. Y., Abidin, I. Z., et., Simulation of Edge Cracks Using Pulsed EDDY Current Stimulated Thermography, *Journal of Dynamic Systems, Measurement and Control*, v. 133, 2011.
- [10] Abidin, I. Z., Tian, G. Y., Wilson, J., et al., Quantitative evaluation of angular defects by pulsed eddy current thermography, *NDT&E International*, v. 43, pp. 537-546, 2010.
- [11] Géron, A. "Hands-on machine learning with scikit-learn, Keras and TensorFlow: concepts, tools, and techniques to build intelligent systems. O'Reilly Media, 2019.
- [12] Maslej N., Fattorini, L., Perrault, R., et al., "The AI Index 2024 Annual Report," AI Index Steering Committee, Institute for Human-Centered AI, Stanford University, Stanford, CA, 2024.